Multi-scale measurements of residual stress in a low alloy carbon steel weld clad with IN625 superalloy

G. Benghalia[1], S. Rahimi[1], J. Wood[2], H. Coules[3], S. Paddea[4]

[1] Advanced Forming Research Centre (AFRC), University of Strathclyde, 85 Inchinnan Drive, Inchinnan, PA4 9LJ, UK

[2] Department of Mechanical & Aerospace Engineering, University of Strathclyde, James Weir Building, 75 Montrose Street, Glasgow, G1 1XJ, UK

[3] Department of Mechanical Engineering, University of Bristol, Queen's Building, University Walk, Bristol, BS8 1TR, UK

[4] Stressmap, The Open University, Venables Building, Milton Keynes, MK7 6AA, UK

ABSTRACT

Fatigue fracture is one of the major degradation mechanisms in 4330 low alloy carbon steel pumps utilized in the hydraulic fracturing process operating under cyclic loading conditions. A weld cladding technology has been developed to improve the resistance of these components to fatigue crack initiation, by cladding with a secondary material. This process introduces a residual stress profile into the component that can be potentially detrimental for fatigue performance. The cladding technology under examination is a 4330 low alloy carbon steel substrate weld clad with a nickel-chromium-based superalloy IN625, investigated herein using several experimental residual stress measurement techniques. Understanding the magnitude and distribution of residual stress in weld clad components is of utmost importance to accurately assess the performance of the component in service. This study summarizes the

A peer-reviewed accepted author manuscript of the following in press output: Benghalia, G., Rahimi, S., Wood, J., Coules, H., & Paddea, S. (2017). Multi-scale measurements of residual stress in a low alloy carbon steel weld clad with IN625 superalloy. *Materials Performance and Characterization*.

results of residual stress measurements, using X-Ray diffraction, hole drilling based on electronic speckle pattern interferometry, deep-hole drilling and the contour method, to obtain the residual stress distributions from the surface of the weld clad, through the clad layer and into the substrate material. The results of deep-hole drilling and the contour method show large scale tensile residual stress in the clad layer and compressive residual stress in the majority of the substrate. However, the X-ray diffraction and hole drilling methods indicated the presence of short scale compressive residual stress on the surface and near surface of the clad layer. It was shown that these measurement techniques are complementary in assessing the residual stress profile throughout the entire component.

Keywords: weld cladding; residual stress; X-ray diffraction; hole drilling; electronic speckle pattern interferometry; deep-hole drilling; contour method; 4330; IN625

Introduction

Low alloy carbon steel, such as 4330 investigated herein, is commonly utilised for its' high strength and the ability to achieve an array of properties depending on the microstructure, which can be controlled by cooling rate of the often hot-forged part. Slow furnace cooling or the use of insulation, as opposed to air cooling, decreases the likelihood of stress-induced cracking, whereas intercritical and double hardening heat treatment can result in improved toughness [1], [2]. Regardless of the measures taken to ensure appropriate material properties, the application of the component in operation poses several critical issues. For instance, during the hydraulic fracturing process, the pump bodies, typically made from carbon steel, are subjected to cyclic loading conditions alongside exposure to corrosive media, and are therefore prone to various environmentally assisted degradation mechanisms, such as corrosion and erosion. These mechanisms can greatly reduce fatigue life, as for example 4140 heat treated

steel is shown to experience accelerated fatigue fracture by a factor of 3-4 in a corrosive environment [3]. Although components may be subjected to cyclic loading at stress levels below the yield strength, crack initiation and propagation can occur at applied stresses much lower than the yield point due to stress concentration caused by stress raisers and features in the component's design, or residual stresses remaining in the part from the manufacturing processes. The evaluation of material fatigue performance is crucial for structural integrity, with 90% of service failures in metals being attributed to fatigue-based failures [4].

Weld overlay cladding can be achieved using hot-wire Gas Tungsten Arc Welding (GTAW), depositing a layer of the clad material onto a substrate, creating a bond between the two materials. Manufacturing the entire component using a material with improved corrosion-resistance is unlikely to provide an advantageous solution that is economically feasible. Applying a weld clad material with superior properties on a less resistant substrate is an alternative, economically viable approach to improving mechanical performance and corrosion and erosion resistance, providing an all-encompassing solution for the performance of components operating in such environments. Welding of structures is a common practice, where the welding process typically results in the generation of tensile residual stress that can have negative effects on the performance and structural integrity of the structure by providing sufficient driving force for crack initiation and propagation [5]. The presence of a compressive residual stress can improve stress-corrosion cracking resistance and corrosion performance [6], as well as increasing fatigue strength [7]. Shortening of the crack initiation stage is a danger of welding processes, along with modification of the material properties of the substrate.

Residual stresses, present in a part in the absence of external applied loads or constraints, arise from misfits between different regions such as heterogeneous plastic

deformations, different crystallographic structures and thermal expansion coefficients [8]. The magnitude and distribution of these self-equilibrating elastic stresses requires knowledge of the key process variables experienced by the component during manufacture, for example heat treatment [9], mechanical work [10], heterogeneous plastic deformation [11], [12] or welding [13]. Thermal expansion constraints and non-uniform heating and cooling all induce residual stresses of different scales, and thus processes such as forging, quenching, welding and brazing cause dissimilarity in the material [14]. Likewise, chemical reactions, volume changes and phase transformations either generate residual stress or influence the existing residual stress field [15]–[17]. Residual stresses can be categorised as macro and micro residual stresses; macro stresses being those with wavelengths comparable to the size of the component, whilst micro stresses are in the region of grain and atomic scales [7]. Both macro and micro stresses may be present in a component, the former also classified as Type I and the latter divided into Type II (i.e. at grain level) and III (i.e. at atomic level) residual stresses.

In weld cladding, residual stress will arise due to mechanical, thermal and chemical mechanisms with the resulting microstructure and in turn the nature of residual stress dependent on the degree of material dissimilarity [18]. It is common for welding and similar thermal processes to induce a complex residual stress field, with potentially sharp stress gradients [19]–[21]. Thermally-induced residual stress is generated due to the non-uniform heating and cooling operations during welding, resulting in constraint on thermal expansion and contraction. At a microscopic level, a mismatch between coefficients of thermal expansion and coherency of the crystallographic structures of the neighbouring phases will contribute to the development of thermally-induced residual stress [22]. A global ‘shrink-fit’ effect occurs between clad and substrate materials, influenced by the material and temperature dissimilarity [23], [24]. Chemically generated residual stresses can develop due to volume changes

associated with chemical reactions, phase transformation and microstructural evolution, such as precipitation hardening [22]. Often such factors are observed through their influence on material properties and ultimately the resulting nature of residual stress [14], [25]. Lastly, the spatial and temporal variation of the clad deposition process and subsequent cooling rate of the component also contributes to the residual stress state [26]. Variation in the temperature of clad and substrate materials affects cooling rates and in turn constraint levels in the component. Material properties vary with temperature and time and therefore the thermal transient process arising is heavily dependent on the differing expansion and contraction rates. During cooling, yield strength and Young's modulus develop, with values differing in neighbouring regions hence the resulting variation in thermal stress [27]–[29].

Improvement in fatigue life is often investigated through examining the residual stress state and methods of beneficially altering the residual stress state. However, many investigations into the welding or cladding of IN625 focus on microstructural evolution, material properties and often corrosion resistance [18], [30]–[37]. This is of particular interest in the region where operational stresses are highest, commonly at the surface of a component or structure. Upon superimposing residual and operational stresses, ideally the entire stress cycle would remain in the compressive range. However, any level of compressive residual stress would be beneficial in lowering the combined stress level. An in-depth understanding of the effects of the welding process on the residual stress state, material properties and fatigue performance of the component is required, this forming the basis of this research.

In this study, a 4330 low alloy carbon steel weld clad with IN625 nickel-based superalloy has been investigated to deduce the magnitude and distribution of residual stress induced by the cladding process. This includes surface, near-surface and bulk residual stress

through the clad layer to the base material, using different measurement techniques. These are X-Ray Diffraction (XRD), hole drilling based on electronic speckle pattern interferometry (ESPI), deep-hole drilling (DHD) and the contour method (CM). A variety of residual stress measurement techniques are well presented by Kandil [5] highlighting practical, material and physical considerations as well as the advantages and disadvantages of the techniques. These methods are complementary and therefore a measurement program such as that presented herein is required to gain an accurate understanding of the residual stress distribution throughout a component. Comparisons have been made between the results of XRD and ESPI for surface residual stresses, and DHD and CM for through-thickness residual stresses.

Experimental Procedure

MATERIAL AND PROCESSING

The material chosen for this investigation is 4330 low alloy carbon steel in the form of a hollow cylinder. A schematic representation of the specimen dimension labels and measurement locations are shown in

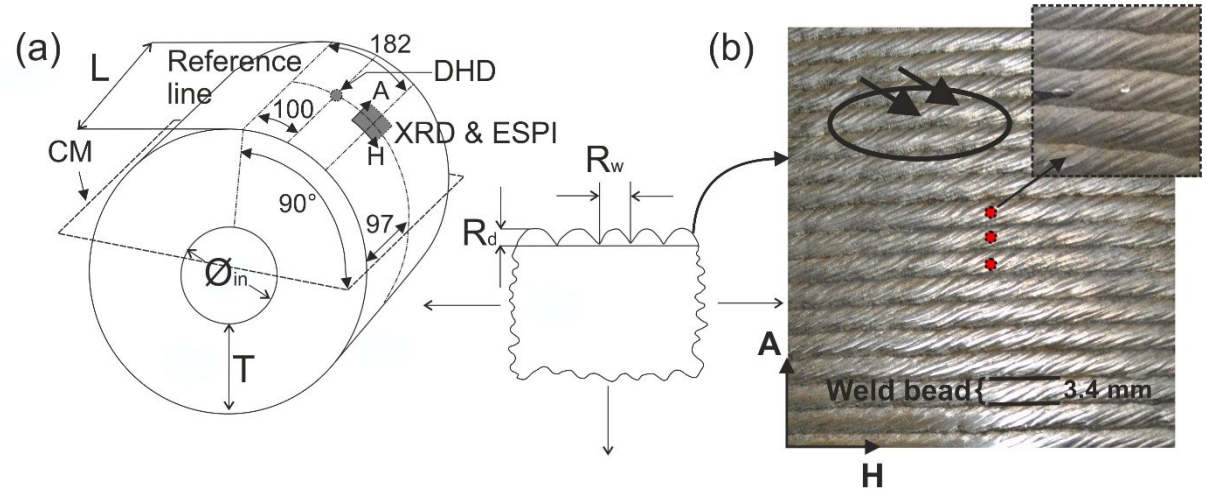

FIG**. 1** and measured values presented in TABLE 1. Weld overlay cladding of the cylinder was achieved using hot-wire Gas Tungsten Arc Welding (GTAW) to deposit a layer of IN625 onto the outer diameter of the 4330 steel hollow cylinder. The outer diameter was selected for

deposition of the clad layer as it was deemed that the nature of residual stresses would be similar on both the inner and outer diameters due to the large thickness of the cylinder in comparison with the clad layer thickness. This thereby facilitated simpler deposition of the clad material and in turn allowed residual stress measurements using a variety of techniques; both aspects experiencing increased complexity and limitations had the clad layer been deposited on the bore. The weld cladding process created a bond between the base and the cladding material, with a periodicity of 1 bead per 3.40 mm. Each bead is composed of approximately 2 small weld ripple pockets per 4.74 mm oriented within 161.46 ± 6.56 ° of the specimen's radial direction (see

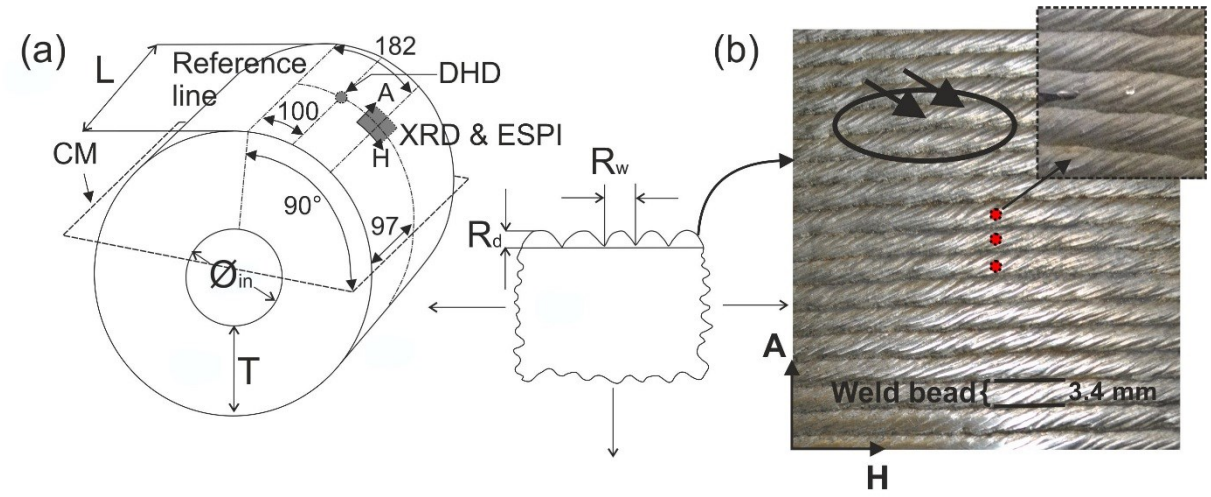

FIG**. 1**b). A two-pass deposition process was utilised resulting in a total clad layer thickness of 6 mm. The nominal chemical composition of substrate and clad materials are summarised in TABLE 2. A single cylinder was utilised for all residual stress measurements that will be presented in the following section. Measurement locations were selected with consideration of accuracy of measurements, hence for example, the surface utilised for deep-hole drilling was an intact surface as opposed to the location at which a hole had been drilled for a hole drilling measurement.

RESIDUAL STRESS MEASUREMENT

X-Ray Diffraction

Surface residual stress measurements were obtained using X-ray diffraction (XRD), utilising a PROTO-LXRD diffractometer and the $sin^2\psi$ method [38]. Stresses were calculated from the strains of the {311} Bragg reflection, assuming elastic Young's modulus of E =168 GPa according to the experimental measurement of this property in the clad layer and Poisson's ratio of ν = 0.29. A Mn K-α target tube was utilised with a wavelength of 2.1031 Å. Measurements were obtained at psi offset angles of 0°, ±4.36°, ±13.6°, ±18.69°, ±24.48° and ±30°, with a ±3° oscillation at each angle and an angle of ±13.6° between the beam and each detector. Measurements were undertaken utilising a 2 mm round collimator, as highlighted in FIG. 2, in two perpendicular directions: axial, along the length of the cylinder (φ = 0˚) and hoop, tangential to the surface of the cylinder (φ = 90˚). Two extra measurements were also performed at φ = 60˚ and φ = -23˚, respectively representing the directions parallel and perpendicular to a striation (i.e. weld ripple pockets) in the weld bead. These angles are schematically illustrated in FIG. 2b. It should be noted that due to the irregularity of the weld clad deposition, care was exercised to ensure the most appropriate definition of the directions parallel and perpendicular to the striation and hence these values depend on measurement location and cannot merely be considered as mathematically perpendicular i.e. at 90° to one another. Consideration of the beam diameter ensured that all measurements were obtained solely across one weld bead, however, curvature of the weld bead was unavoidable as illustrated in FIG. 2c.

Measurements were obtained in each case along a path consisting of twenty adjacent weld bead peaks from the reference face of the specimen. The assigned point numbers reflect the weld bead peak numbered from the reference edge.

Hole drilling based on ESPI

A StressTech Prism® system was used for the measurement of residual stress using hole-drilling based on electronic speckle pattern interferometry (ESPI) [39]. The Prism® system consists of a high speed drill, laser source, and a CCD camera. A coherent laser source illuminates the specimen surface with the illumination light, interfering with a separate laser beam originating from the same source as the reference beam, to form a speckle pattern. The low reflectivity of the as-clad surface provided an ideal surface for drilling. Drill diameters determine the depth to which measurements can be obtained; residual stresses obtained to a depth of 60% of the hole size. A drill diameter of 1.8 mm was utilised in this case, ensuring that measurements were not obtained across more than one weld bead. The drill was centered on top of the weld bead in the central weld bead at various locations in the region highlighted in

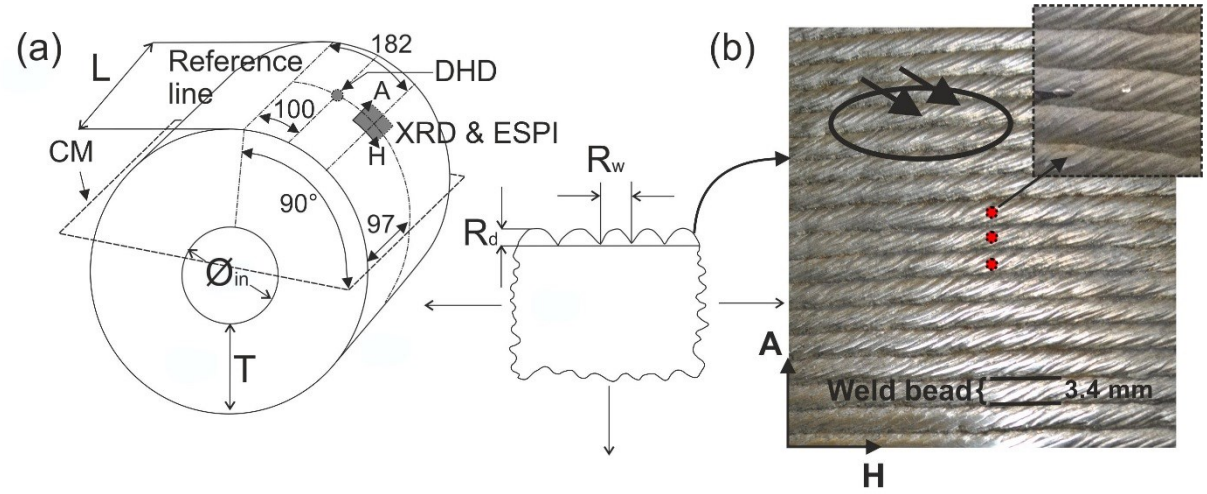

FIG**. 1**b, drilling on the as-clad surface to obtain a quality hole. Residual stresses were calculated from the strains measured by ESPI during incremental drilling, assuming the mechanical properties noted in TABLE 3 for the clad material (i.e. IN625).

Deep-hole drilling

Deep-hole drilling (DHD) measures strain relief through the drilling of a reference hole and an electro-discharge machine (EDM) trepanned core comparing differing diameters due to mechanical relaxation. Converting measured strains and using elastic theory, residual stresses are obtained through the thickness of the component. The trepanning of the hole during

measurement causes the release of residual stress in the vicinity of the trepanned region, with the displacement [δ] described in relation to the original stress through the following equation [40]:

$$[\delta] = -\frac{1}{E}[D][\sigma] \quad \text{Equation 1}$$

In this equation, E is the Young's modulus and [D] a matrix relating to the hole edge displacement in a stressed plate, the theory of DHD being well described in various studies [41]–[43].

DHD was performed using a reference hole drilled in the cylinder's radial direction from the clad surface to the bore. The reference hole was located half-way along the cylinder's axis. This enabled measurement of the axial, circumferential, and axial-circumferential shear components of the residual stress at the reference hole location as a function of through-wall depth. The reference hole had a nominal diameter of 3 mm and was incrementally stress-relieved using a coaxial EDM trepan with a diameter of 10 mm.

Measurement of the reference hole was performed at trepanning increments of 2.5 mm up to a depth of 20 mm, and again after trepanning to the full depth of the hole. In each measurement, the reference hole diameter was determined at angular increments of 22.5° every 0.2 mm between the clad surface and the pipe bore, using an air probe. Residual stresses were calculated from measured diametral displacements using Equation 1 above. In this calculation differing elastic properties were used for the IN625 cladding material and the 4330 cylinder wall material, as given in TABLE 3. Results from the incremental trepanning steps indicated that no significant plasticity occurred close to the reference hole during the measurement, so

the incremental analysis procedure described by Mahmoudi et al. [42] was not required.

Contour method

The contour method provides a 2D map of out-of-plane residual stress in the cut direction through sectioning of the component, using Bueckner's superposition principal [44]. The first cut in the axial plane, shown in

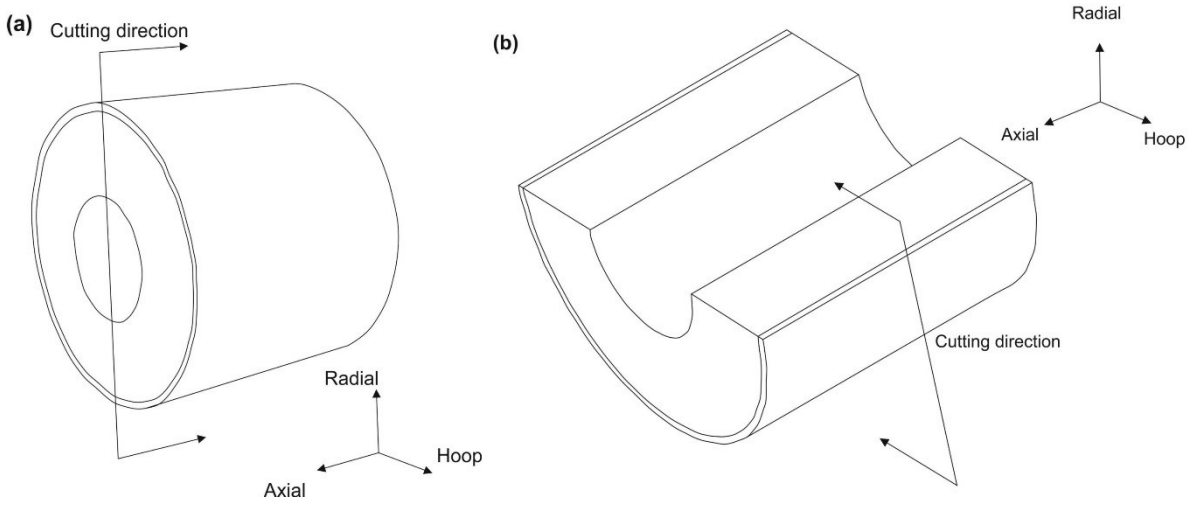

FIG**. 3** provides the hoop residual stress with the second cut in the hoop plane providing the axial residual stress.

The contour method was carried out on the clad cylinder to provide a full 2D map of both hoop and axial residual stress distributions in the sample. For the hoop residual stress, the contour method included the release of bending moments, as described by Prime [45], which act as an additional source of hoop residual stress. The measurement of each stress component was carried out in four main steps of sample cut, measurement of cut surface profiles, data processing, and calculation of residual stress using finite element simulation.

EDM wire entry and exit from the test specimen can introduce cutting artefacts that affect near surface measurements. Wire entry refers to the top face of the specimen where the running wire enters the test specimen. Wire exit relates to the bottom face of the specimen where the running wire leaves the test specimen. To mitigate wire entry and exit cutting

artefacts, sacrificial layers were bonded on the top and bottom faces of the pipe and the bore in the vicinity of the cut plane [46]. The cuts were made by electrical discharge machining (EDM) using a 250 µm brass wire in 'skim' cut mode. For the hoop stress component, the cut was made in the axial direction on the axial-radial plane (

Axial

FIG. 3a) covering the entire part, starting from one end to another. Prior to sectioning, two pilot holes with 3mm diameter, were drilled at approximately 5mm distance from both ends of the pipe, such that the cut was conducted from the centre of a hole on one side to the centre of the hole on the other side of the part, aiming to cut the test specimen using an embedded cutting configuration. The advantage of this technique is that it provides self-constraint which restricts opening of the cut faces, thereby controlling the stress concentration and reducing the risk of significant plasticity arising at the cut tip during cutting. Following the completion of the cut, the remaining ligaments were severed to separate both halves of the part.

A single contour cut [47] was used to determine the distribution of hoop stresses on an axial-radial plane bisecting the clad pipe, that is simultaneously mapping the hoop stresses on two wall thicknesses 180° apart. Moreover the measured stress field included the effect of hoop bending stresses and their variation along the pipe. This approach has several advantages over that of Prime [45]; a single cut is required (instead of three cuts), stresses in diametrically opposite sides of the pipe are determined (compared with stresses on a single side) and any variation in hoop bending stresses, if present, along the length of the pipe are captured.

For the axial stress component, the contour method residual stress measurement was conducted on one half of the part, as shown in

Axial

FIG. 3b. Again, sacrificial materials were bonded to the inner and outer diameters to create a uniform cross-section. Since the contour method measurement on one half can only provide the partial axial residual stress component, the total axial stress is obtained through the principal

of superposition, expressed in Equation 2:

$$\sigma_{\text{Axial,total}} = \sigma_{\text{Axial,relaxed}} + \sigma_{\text{Axial,remaining}} \quad \text{Equation 2}$$

Where, the relaxed axial stress arises due to the first cut undertaken to measure the hoop stress and the remaining axial stress being due to the second contour cut [48], [49].

Upon completion of the EDM cuts, the outline and surface topography were measured for each cut on either side of the skim cut in a temperature controlled environment using a laser hybrid coordinate measuring machine (CMM). The CMM equipment was programmed to acquire data with a spatial resolution of 100 μm for points in both in-plane directions.

The measured data obtained for both surfaces of each skim cut was aligned in the same coordinate system by considering the whole perimeter of each half of the cut as an alignment guide to match the outlines. Following the alignment process, the datasets for both sides were linearly interpolated onto a common grid, after which the two sets were averaged. Noise and outliers in the averaged dataset are then removed before smoothing the data. A knot spacing of 1 mm^2 was selected for the calculation of hoop and axial stress and a bivariate cubic spline for each knot spacing fitted to the averaged data.

A 3D finite element (FE) model assuming isotropic elasticity, with a Young's modulus of 168 GPa and 189.8 GPa and a Poisson's ratio of 0.29 and 0.289 for the clad and substrate materials respectively, was used to evaluate the residual stress from the surface contour data. For this purpose, the perimeter of the cross-section for each sample was modelled using the aligned outline measured by the CMM. The 2D cross-section was then revolved

circumferentially by 180° for the hoop stress component, and extruded to the length of the cylinder, 250 mm, for the axial stress component, producing 3D models for the calculations of residual stress. Mesh seeds were attributed to each node on the outline and along the revolved and extruded perimeters of the models that are used as guidelines for the generation of mesh. The establishment of the seeds were biased by allocating a finer pitch near the cross-section of the model representing the cut surface, and coarser pitch towards the other end of the model, of less importance for stress analysis. The parts were modelled in Abaqus CAE and meshed with a fine mesh of 0.4 mm in the clad layer and 4 mm towards the inner diameter. For the residual stress model, the stresses were calculated by forcing the cut surface into the opposite shape of the averaged contour data [19], [50], [51].

Results

X-RAY DIFFRACTION

FIG. 4 illustrates the presence of variations in measured residual stress magnitudes in both the axial and hoop stress components on the as-clad surface, with the majority of measurements and the average values being compressive in nature. The uncertainty for each measurement point is evaluated based on the best fit to the $sin^2\psi$ method. The average values are calculated by averaging the stresses measured for all points, and their associated uncertainties were calculated through taking the second root of the sum of the squares of the uncertainties of all points evaluated by $sin^2\psi$ method.

HOLE DRILLING BASED ON ESPI

Depth profiles of residual stress distribution quantified by hole-drilling based on ESPI for different weld beads are provided in

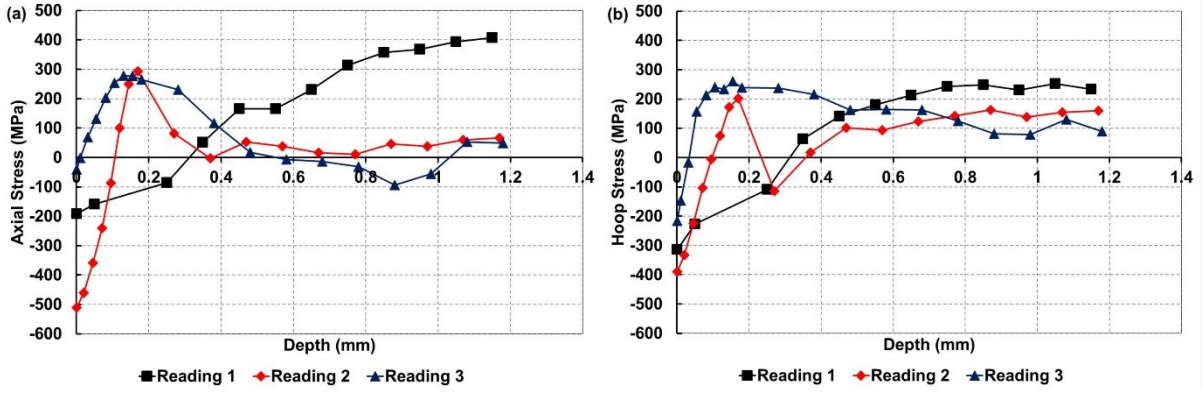

FIG. **5**, displaying the data obtained for both hoop and axial directions. The measured hoop and axial components indicate the presence of compressive residual stress with a maximum of -390 MPa and -511 MPa, respectively, on the surface. These are then reduced to a stress-free state in both directions at a depth of approximately 0.3-0.5 mm in most cases, at which point the nature of stress tends to transform to tensile. Both hoop and axial stress components increase in a tensile manner deeper into the clad layer, to a maximum of +233 MPa and +407 MPa at a depth of 1.2 mm, respectively. Given the 1.8 mm drill diameter utilised, residual stress was measured to a depth of 1.2 mm. Offset depths are utilised here, indicating the beginning of a measurement at an effective zero depth through the removal of material to reveal a complete circle. However, clearly for the means of comparison with other methods, depth from the clad surface will be used in the later comparisons.

DEEP-HOLE DRILLING (DHD)

FIG. 6a illustrates the hoop and axial residual stresses throughout the section, indicating that the general trend and nature of residual stress are similar for both components. Tensile residual stresses with magnitudes of +212±20 MPa and +243±20 MPa are present on the

surface for hoop and axial components respectively, reducing to 0 MPa at a depth of 12-15 mm depending on direction. Due to the self-equilibrating nature of residual stress, compressive stresses are measured further into the substrate, counterbalancing the tensile stresses on the surface.

FIG. 6b presents the results concentrating on the vicinity of the join between clad and substrate materials. Beyond a depth of 5 mm, it can be seen that a smoother profile emerges, illustrating the change between clad and substrate materials. At the interface there is no sharp discontinuity present as was illustrated in modelling results previously [52]. Such discontinuity stresses were expected to be exaggerated due to the idealised interface modelled, not accounting for alloying and diffusion due to the weld cladding process [53]. A slight increase in tensile residual stress occurs immediately upon entering the substrate material, prior to a decrease into the compressive region. Small levels of compressive residual stress exist between 15-20 mm from the outer diameter indicating that indeed alloying and diffusion successfully smooth potential stress discontinuities arising due to dissimilar materials.

CONTOUR METHOD

FIG. 7 and

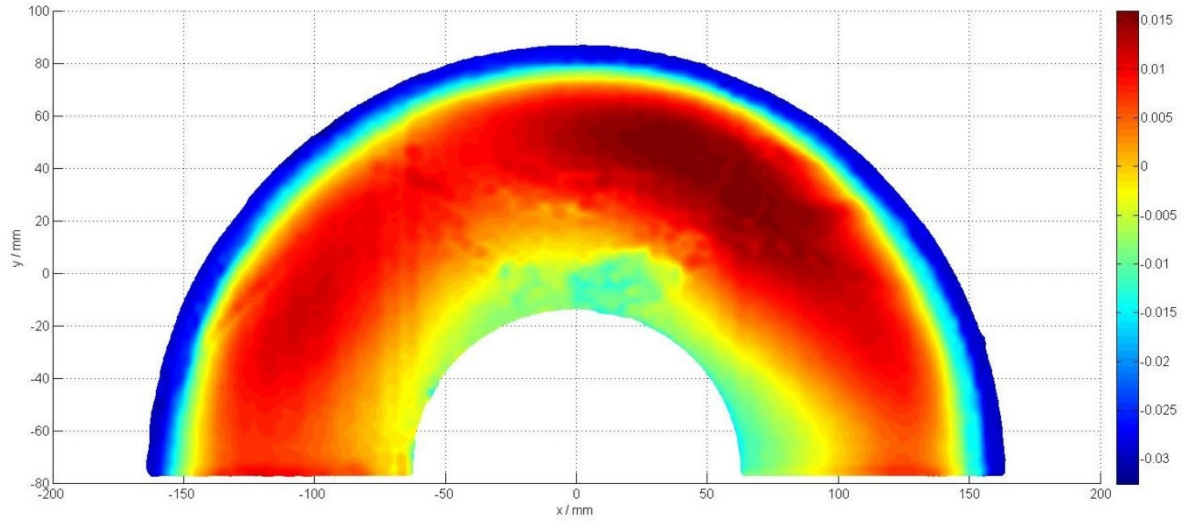

FIG. **8** show the contour plots of the averaged surface height obtained by the CMM following the EDM skim cut for both hoop and axial stress measurements respectively. The range of peak to valley of the contours exceeds 120 µm for the hoop component and 45 µm for the axial. The contour plots show that the surface height for both directions is low in the weld region implying that tensile residual stresses are relieved.

The contour plot of the out-of-plane hoop residual stress measured on the sectioned surface is shown in FIG. 9. This plot illustrates a consistent pattern from the clad surface into the substrate to the bore. From the hoop stress map provided in FIG. 9, it can be seen that tensile residual stresses (i.e. green to red) were largely concentrated within the clad layer and the heat affected zones, in the interference zone between the clad and the substrate. Hoop residual stress profiles are presented in FIG. 10 for 6 chosen paths highlighted in FIG. 9, emphasising the clad layer and the substrate interface in FIG. 10b. The region of highest tensile residual stress was identified immediately at the clad surface, with the peak stress reaching +677 MPa, as shown in the data for path 1 in FIG. 10b.

FIG. 10a shows a high tensile residual stress at the clad layer surface followed by a decrease to a notable compressive residual stress. An increase to tensile residual stress remains to a depth of around 15 mm, with compressive residual stresses then emerging in the substrate, similar to those measured by DHD.

Focusing on a region in the vicinity of the join, shown in FIG. 10b, the data shows compressive residual stress at a depth of 2 mm ranging between -316 MPa and +72 MPa for the various paths. Such variations are thought to be due to the spatial weld cladding process and weld bead peak and trough effects, resulting in varying residual stress distributions along the length of the cylinder as highlighted in FIG. 9. It should also be noted that the various methods utilized herein have varying degrees of spatial resolution, and the spatial resolution requirements should always be considered during technique selection [7], [54]. In this study, it is highlighted that only through the complementary use of XRD, ESPI, DHD and CM has a detailed residual stress distribution been obtained both in the weld clad layer and throughout the component.

Axial residual stresses superimposed for the relaxed stresses of the first cut and the remaining measured stresses of the second cut produces the stress map shown in FIG. 11. The plots of the three lines in FIG. 11 indicates (see FIG. 12) that the axial stress possesses a much smoother nature than the hoop stress component, with a consistent tensile residual stress in the clad layer continuing into the substrate. Compressive axial stress is measured in the substrate

to a similar level as that measured by DHD.

Discussion

The following section presents a comparison of results obtained using all measurement techniques along with a discussion of the considerations relating to the obtained residual stress distributions.

COMPARISON OF SURFACE AND NEAR-SURFACE RESIDUAL STRESS

Surface and near-surface residual stresses were measured using XRD and hole-drilling method based on ESPI, respectively. The penetration depth of the X-ray used in these measurements is approximately 10 μm in IN625, while the ESPI measurements are obtained incrementally from a depth of 20-50 μm from the surface to a depth dependent on the level of material removed to reveal a complete circle. Therefore, these methods are complementary in constructing the residual stress profile in the surface region.

XRD measurements obtained on weld bead peaks did not provide wholly consistent results, as shown in FIG. 4. This may be due to a slight difference in the positioning of the X-ray beam on the weld bead, and also variation in the number and morphology of the weld ripple pockets (i.e. striations) covered by the beam. If the beam is not perpendicular with the peak of the weld bead, then stress values may vary significantly [38]. Axial and hoop stress values appear to have been potentially influenced by these factors. FIG. 4b suggests that generally towards the edge of the cylinder, hoop stresses are tensile, whilst further from the edge of the cylinder compressive stresses are measured. However, this does not appear to be the case for axial stresses shown in FIG. 4a, being largely compressive regardless of distance from the

reference face. The error is calculated as a best fit to the $sin^2\psi$ method and hence larger error values may manifest due to striation effects, surface irregularities, large grain sizes and texture. Error values also differ greatly between point measurements, likely due to the curvature [38] of the weld bead if deviation from a perpendicular beam to surface condition occurs. The X-ray beam did not extend across more than one weld bead, however, the beam may deviate from normal to the weld bead depending on the measurement surface (i.e. the curved bead).

Strain values are averaged across the measurement region and therefore calculated stress values are also affected. Geometrical variations and surface irregularities could also lead to inaccuracies in stress values [38]. The surface profile and weld bead geometry will vary across the cylinder, potentially affecting stress values. As highlighted in FIG. 4, the majority of axial and hoop residual stress values along with average values obtained using XRD on the weld bead peaks were compressive. Inconsistencies in the measurements obtained using XRD alone proves the difficulty in comparing residual stress measurement methods. However, this is not due to inaccuracy of the measurement technique but due to the technique identifying varying levels of residual stress due to the weld bead geometry.

ESPI also indicated compressive residual stresses immediately at the clad layer surface (i.e. near-surface residual stress). These compressive residual stresses were similar in magnitude (i.e. within 3 MPa for the axial stress component and 166 MPa in the best case comparison) to those obtained using XRD. ESPI then showed a transformation into tensile residual stress in both hoop and axial stress components at a depth of 0.3 mm, after which the level of tensile stress increased to +233 MPa and +407 MPa at the furthest depth of measurement obtained. The presence of compressive residual stresses on the surface and near-surface is a characteristic of fast cooling from elevated temperatures that happens immediately after the weld is embedded. The high heat exchange rate between the hot surface and the environment leads to a differential contraction and expansion between a cold surface and hot interior at the early stages of cooling that can plastically deform the surface [8]. Subsequently, when the entire part is cooled down to room temperature, the plastically deformed surface is forced by the bulk interior material to a location and condition that generates compressive residual stress [12]. Due to the self-equilibrating nature of residual stress, an area immediately below the plastically deformed surface develops tensile stress to counterbalance the

compressive stress on the surface. This has been seen in this study, as shown in

Depth from clad surface (mm) Depth from clad surface (mm)

FIG**. 13**b and FIG. 14b. The presence of a compressive residual stress is particularly beneficial at the surface of a component where operational stresses are often highest. Upon super-positioning of the residual stresses with cyclic operational stresses, the entire stress cycle would ideally remain in the compressive region and in turn crack propagation tends not to occur [5], [25], [55], [56]. Crack initiation is, however, thought to be uninfluenced by the presence of compressive residual stress [42], or can be enhanced by type III residual stress [57]. Compressive residual stress can also improve corrosion performance and stress corrosion cracking performance for some materials [30], [57], [58].

COMPARISON OF THROUGH-THICKNESS RESIDUAL STRESS

The compressive residual stress obtained directly at the surface using XRD and ESPI are complementary to the data measured by DHD and the CM to reconstruct the full stress profile from the surface through the clad layer and into the bulk material. Both DHD and CM techniques measured tensile residual stress close to the surface, in reasonable proximity to the data obtained by ESPI. The air probe used in the DHD method cannot measure accurately at depths of less than ≈1 mm from the surface, leading to the loss of stress information at the surface and near-surface. This information is measured by the XRD and ESPI based hole-drilling (see

Depth from clad surface (mm) Depth from clad surface (mm)

FIG**. 13** and FIG. 14). The data shows that different measurement techniques can detect variations in residual stress, however, not to the same resolution despite all considering for the measurement of Type I residual stress. This is of the greatest differentiating factor between the surface, near-surface and through-section measurement techniques. Clearly, the results are also location dependent and as such, the discrepancies arising in comparative figures is to be expected given that locations differ. It is further noted that in CM results, as has been illustrated, the level of residual stress measured at the surface and into the clad layer is dependent on the path through which stresses are plotted. This can be due to slight variations in the residual stress distribution in the axial direction, perhaps due to the weld cladding process or consequent

cooling, although CM can also struggle to provide details of residual stress close to the edges should cutting artefacts be present [46].

In comparing DHD and CM results, residual stress to a greater depth within the component can be evaluated. Axial and hoop residual stresses are shown for both methods in FIG. **13** and FIG. 14 respectively. The data plotted for the contour method is the average for both axial and hoop stresses (FIG. 12 and FIG. 10). Comparing these results illustrates that stress distributions obtained are comparable in general, with large tensile residual stresses close to the clad layer surface, tending to decrease towards the interface. Compressive residual stresses are observed in the substrate for both measurement techniques and both stress components, prior to a transformation into tensile residual stresses at the cylinder bore. At a depth of 2 mm in the hoop component there is a discrepancy with stress levels in the CM results decreasing into the compressive region, highlighted clearly in FIG. 14b. Through decreasing the knot spacing increased accuracy could be achieved in such regions, but in turn the noise in the measurement increases. Therefore, care must be taken when selecting the parameters for calculation of the residual stress to ensure that sufficient detail is obtained whilst minimising data noise [59]. Stress values obtained using DHD are supported by those of ESPI with tensile residual stresses of +274 MPa obtained at a depth of 1.2 mm, compared with +233 MPa obtained using ESPI. Upon the stress level of CM data reaching a high tensile residual stress once more, the data for DHD and CM is similar.

Depth from clad surface (mm)

Depth from clad surface (mm)

Comparing the residual stresses measured on the surface, near-surface and through-thickness, it is clear that there are surface effects due to the geometry of the weld bead influencing the residual stress immediately at the surface that cannot be measured by both DHD and CM. This is particularly because DHD requires surface preparation that results in the elimination of surface and near surface stress data, while CM results may be subject to cutting artefacts. Furthermore, surface irregularities caused by the weld bead peaks and troughs along with weld pass effects present complexities in evaluating the residual stress with high sensitivity such that these cannot be precisely measured by the laser CMM. This in turn increases the uncertainty associated with the finite element simulation and application of the superimposition principle of contour method. The average peak to trough measurement was

0.35 mm as noted in TABLE 1 and this was not considered in the contour method measurement. Hence the weld surface edge in FIG. 9 appears as a straight line whereas in reality it is a 'serrated' edge is as shown in
"
FIG**. 1**. Various studies have shown that the weld bead geometry and behavior has a great impact on resulting residual stress [60]–[62]. This may well explain the decrease into the compressive region in the hoop stress component measured by CM in the clad layer. Therefore, the compressive residual stresses measured at the weld clad surface and near surface by XRD and ESPI are providing complimentary data to those measured by DHD and CM.

CLADDING INDUCED RESIDUAL STRESS

During the course of this study, the greatest driver in material and process selection, was to obtain a material combination that would generate compressive residual stress through weld cladding, particularly at the surface, the location at which operational stresses are highest.

In this paper, weld cladding of 4330 low alloy carbon steel has been carried out using nickel chromium-based superalloy IN625. Corrosion resistance offered by this alloy is advantageous, however, the tensile residual stress present in the clad layer will not aid in increasing resistance to fatigue-failure [16], [63].

The residual stress distribution obtained when weld cladding a 4330 low alloy carbon steel substrate with 17-4 PH stainless steel has indicated the potential of obtaining compressive residual stress in the clad layer [21]. This indicates that material selection and the consequent interaction between clad and substrate materials is a key factor in the resulting residual stress distribution and in turn the effects on fatigue performance.

The mechanisms involved in the weld cladding process, including mechanical, thermal

and chemical mechanisms, give rise to residual stresses due to the joining of dissimilar materials, resulting in a complex residual stress distribution. The 'shrink-fit' effect occurring due to the shrinkage of the cladding relative to the substrate can give rise to varying residual stress levels in the vicinity of the join due to variations in the heating and cooling cycle occurring during welding [7]. This in turn results in varying levels of constraint on thermal expansion and contraction and on a microscopic level, varying values of thermal properties in constituent phases that can generate varying residual strain fields [8]. This effect can be observed in the locations of maximum tensile and compressive residual stresses (see TABLE 4 and TABLE 5, respectively), primarily in the XRD results. It can be seen that maximum surface residual stresses measured are high in both tensile and compressive cases, particularly in the case of compressive residual stresses. This highlights that significant variations in stress levels can be observed using XRD, whether these are due to the residual stress generation mechanisms or measurement considerations. Joining of the materials can alter material properties and microstructures through alloying and diffusion, giving rise to variations in residual stress depending on measurement location in the clad layer or in the vicinity of the join [64]. It should be highlighted that residual stress present in the original cylinder prior to cladding should not be neglected and that a stress-relief process should ideally be undertaken. Failing this, simulation of the residual stress due to forging, cutting and machining should be carried out to quantify the stress-state prior to cladding. Maximum tensile hoop and axial residual stresses have been observed in the clad layer for all methods, however, discrepancies arise in the compressive stress component (TABLE 5). Variations could also arise due to the spatial and temporal variation in the cladding process and therefore the location selected for measurement may not be fully representative of the entire component [26]. Such potential effects on the residual stress state in a component highlight the need for a highly controlled and optimised deposition process and subsequent cooling to ensure residual stress generation is not

only understood but also, repeatable.

Although IN625 is a commonly utilised material in weld cladding, the tensile residual stress generated in the clad layer means that from this perspective there is potential for improvement to achieve an all-encompassing solution for a corrosion and erosion resistant component with a favourable residual stress state. A tensile residual stress increases the mean stress and this will in turn increase the maximum stress level reached during service. In cyclic loading conditions, each cycle will cause an increase in fatigue damage through crack growth [65], [66]. This will continue until the critical crack length results, leading then to crack propagation and component failure. For this reason, the presence of compressive residual stress is desired, such that crack growth will be limited due to the lack of the tendency of the crack face to open during cyclic stress conditions.

Conclusions

In this study, detailed analyses of residual stress distributions in a 4330 low alloy carbon steel cylinder weld clad with nickel chromium-based superalloy IN625 were obtained. The major observations of this work are concluded as follows:

- The weld cladding of a 4330 low alloy carbon steel cylinder with nickel chromium-based superalloy IN625 is achieved using a hot-wire GTAW process. A clad layer is deposited on the outer diameter of the cylinder in two passes, resulting in a 6 mm deep clad layer.
- The residual stresses throughout the component are measured using different techniques, including XRD, hole drilling based on ESPI, deep-hole drilling and the

contour method. These methods are shown to be highly complementary, gaining detailed residual stress distributions resulting from the weld cladding process.

- XRD and ESPI methods indicate compressive residual stresses present at the clad layer surface, to a depth of around 0.35 mm as indicated by ESPI. Hole-drilling based on ESPI, deep-hole drilling and the contour method indicate that further into the clad layer tensile residual stresses are present. Deep-hole drilling and the contour method allow the distribution throughout the clad layer, at the interface and throughout the substrate to be measured. It is shown that a balancing of the tensile residual stresses occurs with the presence of compressive residual stresses in the substrate. Both hoop and axial stress components are consistently the same in nature, with similar levels of stress throughout.
- The study highlights the need for a range of residual stress measurement techniques to gain knowledge of the residual stress distribution throughout the component.
- Weld cladding with IN625 has resulted in the presence of compressive residual stress on the surface and near surface, counterbalanced by tensile residual stresses at greater depths.

ACKNOWLEDGEMENTS

The authors would like to acknowledge the support provided by the Weir Advanced Research Centre for the manufacture of the weld clad cylinder. The experimental works were carried out primarily at the Advanced Forming Research Centre (AFRC), University of Strathclyde, which receives partial financial support from the UK's High Value Manufacturing CATAPULT.

REFERENCES

[1] L. Shi, Z. Yan, Y. Liu, C. Zhang, Z. Qiao, B. Ning, and H. Li, "Improved toughness and

ductility in ferrite/acicular ferrite dual-phase steel through intercritical heat treatment," *Mater. Sci. Eng. A*, vol. 590, pp. 7–15, 2014.

[2] K. Srivatsa, P. Srinivas, G. Balachandran, and V. Balasubramanian, "Improvement of impact toughness by modified hot working and heat treatment in 13%Cr martensitic stainless steel," *Mater. Sci. Eng. A*, vol. 677, pp. 240–251, 2016.

[3] K. Genel, M. Demirkol, and T. Guelmez, "Corrosion Fatigue Behaviour of Ion Nitrided AISI 4140 Steel," *Mater. Sci. Eng. A*, vol. 288, pp. 91–100, 2000.

[4] W. F. Hosford, *Mechanical Behavior of Materials*. Cambridge, UK: Cambridge University Press, 2005.

[5] G. A. Webster and A. N. Ezeilo, "Residual stress distributions and their influence on fatigue lifetimes," *Int. J. Fatigue*, vol. 23, pp. 375–383, 2001.

[6] A. F. Liu, *Mechanics and Mechanisms of Fracture: An Introduction*. Ohio, USA: ASM International, 2005.

[7] F. A. Kandil, J. D. Lord, A. T. Fry, and P. V. Grant, *A Review of Residual Stress Measurement Methods - A Guide to Technique Selection*. Teddington, UK: National Physical Laboratory, 2001.

[8] P. J. Withers and H. K. D. H. Bhadeshia, "Residual Stress: Part 2 - Nature and Origins," *Mater. Sci. Technol.*, vol. 17, no. April, pp. 366–375, 2001.

[9] R. H. Leggatt, "Residual stresses in welded structures," *Int. J. Press. Vessel. Pip.*, vol. 85, no. 3, pp. 144–151, Mar. 2008.

[10] N. Stenberg and J. Proudian, “Numerical modelling of turning to find residual stresses,” *Procedia CIRP*, vol. 8, pp. 258–264, 2013.

[11] Z. Zhang, Y. Yang, L. Li, B. Chen, and H. Tian, “Assessment of residual stress of 7050-T7452 aluminum alloy forging using the contour method,” *Mater. Sci. Eng. A*, vol. 644, pp. 61–68, 2015.

[12] D. Dye, K. T. Conlon, and R. C. Reed, “Characterization and modeling of quenching-induced residual stresses in the nickel-based superalloy IN718,” *Metall. Mater. Trans. A*, vol. 35A, no. June, pp. 1703–1713, 2004.

[13] H. E. Coules, “Contemporary approaches to reducing weld-induced residual stress,” *Mater. Sci. Technol.*, vol. 0, no. 0, pp. 1–15, 2012.

[14] V. García Navas, O. Gonzalo, I. Quintana, and T. Pirling, “Residual stresses and structural changes generated at different steps of the manufacturing of gears: Effect of banded structures,” *Mater. Sci. Eng. A*, vol. 528, no. 15, pp. 5146–5157, 2011.

[15] C. R. Li, Z. P. Zhang, Y. M. Zhang, and Z. T. Fang, “Finite Element Simulative Analysis on the Influence of Solid-State Transformation on Welding Residual Stress,” *Adv. Mater. Res.*, vol. 785–786, pp. 1229–1235, Sep. 2013.

[16] T. I. Ramjaun, H. J. Stone, L. Karlsson, M. Gharghouri, K. Dalaei, R. Moat, and H. K. D. H. Bhadeshia, “Surface residual stresses in multipass welds produced using low transformation temperature filler alloys,” *Sci. Technol. Weld. Join.*, vol. 19, no. 7, pp. 623–630, 2014.

[17] T. Nitschke-Pagel and K. Dilger, “Sources and Consequences of Residual Stresses due

to Welding," *Mater. Sci. Forum*, vol. 783–786, pp. 2777–2785, May 2014.

[18] C. C. Silva, H. C. De Miranda, M. F. Motta, J. P. Farias, C. R. M. Afonso, and A. J. Ramirez, "New insight on the solidification path of an alloy 625 weld overlay," *J. Mater. Res. Technol.*, vol. 2, no. 3, pp. 228–237, Jul. 2013.

[19] W. Rae, Z. Lomas, M. Jackson, and S. Rahimi, "Measurements of residual stress and microstructural evolution in electron beam welded Ti-6Al-4V using multiple techniques," *Mater. Charact.*, vol. 132, no. April, pp. 10–19, 2017.

[20] D. Easton, J. Wood, S. Rahimi, A. Galloway, Y. Zhang, and C. Hardie, "Residual Stress Generation in Brazed Tungsten Dissimilar Joints," *IEEE Trans. Plasma Sci.*, vol. 44, no. 9, pp. 1625–1630, 2016.

[21] G. Benghalia, S. Rahimi, and J. Wood, "Measurements of Surface and Near-Surface Residual Stress in 4330 Low Alloy Carbon Steel Weld Clad Components," in *Residual Stresses 2016: ICRS-10*, 2016, pp. 259–264.

[22] S. Rahimi, B. P. Wynne, and T. N. Baker, "Development of Microstructure and Crystallographic Texture in a Double-Sided Friction Stir Welded Microalloyed Steel," *Metall. Mater. Trans. A*, vol. 48, no. 1, pp. 362–378, 2017.

[23] Y. Gexia, "An Analytical Solution of Residual Stresses for Shrink-Fit Two-Layer Cylinders After Autofrettage Based on Actual Material Behavior," *J. Press. Vessel Technol.*, vol. 134, no. 6, p. 61209, Nov. 2012.

[24] A. H. Mahmoudi, G. Zheng, D. J. Smith, C. E. Truman, and M. J. Pavier, "A Procedure to Measure Biaxial Near Yield Residual Stresses Using the Deep Hole Drilling

Technique," *Exp. Mech.*, Feb. 2013.

[25] M. T. Hutchings and A. D. Krawitz, "Measurement of Residual and Applied Stress Using Neutron Diffraction," in *NATO Advanced Research Workshop*, 1991.

[26] B. Taljat, T. Zacharia, X.-L. Wang, J. R. Keiser, R. W. Swindeman, Z. Feng, and M. J. Jirinec, "Numerical Analysis of Residual Stress Distribution in Tubes with Spiral Weld Cladding," *Weld. Res. Suppl.*, no. August, pp. 328–335, 1998.

[27] M. C. Smith, O. Muransky, A. Goodfellow, E. Kingston, P. Freyer, S. Marlette, G. M. Wilkowski, B. Brust, and S. Do-Jun, "The Impact of Key Simulation Variables on Predicted Residual Stresses in Pressuriser Nozzle Dissimilar Metal Weld Mock-ups. Part 2 - Comparison of Simulation and Measurements," *ASME PVP*, pp. 1–17, 2010.

[28] R. J. Dennis, N. A. Leggatt, M. C. Smith, and P. J. Bouchard, "R6 Weld Modelling Guidelines - Application to Groove Weld Worked Example," in *ASME 2010 Pressure Vessels & Piping Division*, 2010, pp. 1–14.

[29] X. K. Zhu and Y. J. Chao, "Effects of temperature-dependent material properties on welding simulation," *Comput. Struct.*, vol. 80, pp. 967–976, May 2002.

[30] S. Liu, W. Liu, M. Harooni, J. Ma, and R. Kovacevic, "Real-time monitoring of laser hot-wire cladding of Inconel 625," *Opt. Laser Technol.*, vol. 62, pp. 124–134, Oct. 2014.

[31] C. A. Maltin, A. M. Galloway, and M. Mweemba, "Microstructural Evolution of Inconel 625 and Inconel 686CPT Weld Metal for Clad Carbon Steel Linepipe Joints: A Comparator Study," *Metall. Mater. Trans. A*, Apr. 2014.

[32] E. Mohammadi Zahrani and A. M. Alfantazi, "Hot Corrosion of Inconel 625 Overlay

Weld Cladding in Smelting Off-Gas Environment," *Metall. Mater. Trans. A*, May 2013.

[33] E. Mohammadi Zahrani and A. M. Alfantazi, "High temperature corrosion and electrochemical behavior of INCONEL 625 weld overlay in PbSO4–Pb3O4–PbCl2–CdO–ZnO molten salt medium," *Corros. Sci.*, vol. 85, pp. 60–76, Aug. 2014.

[34] M. Rozmus-Górnikowska, Ł. Cieniek, M. Blicharski, and J. Kusiński, "Microstructure and Microsegregation of an Inconel 625 Weld Overlay Produced on Steel Pipes by the Cold Metal Transfer Technique," *Arch. Metall. Mater.*, vol. 59, no. 3, pp. 1081–1084, Jan. 2014.

[35] C. C. Silva, C. R. M. Afonso, A. J. Ramirez, M. F. Motta, H. C. De Miranda, and J. P. Farias, "Evaluation of the Corrosion Resistant Weld Cladding Deposited by the TIG Cold Wire Feed Process," *Mater. Sci. Forum*, vol. 783–786, pp. 2822–2827, May 2014.

[36] T. E. Abioye, D. G. McCartney, and A. T. Clare, "Laser cladding of Inconel 625 wire for corrosion protection," *J. Mater. Process. Technol.*, vol. 217, pp. 232–240, 2015.

[37] X. Xing, X. Di, and B. Wang, "The effect of post-weld heat treatment temperature on the microstructure of Inconel 625 deposited metal," *J. Alloys Compd.*, vol. 593, pp. 110–116, 2014.

[38] M. E. Fitzpatrick, A. T. Fry, P. Holdway, F. A. Kandil, J. Shackleton, and L. Suominen, *Measurement Good Practice Guide No. 52: Determination of Residual Stresses by X-Ray Diffraction - Issue 2*, no. 52. Teddington, UK: National Physical Laboratory, 2005.

[39] R. Jones and J. A. Leendertz, "Elastic constant and strain measurements using a three beam speckle pattern interferometer," *J. Phys. E Specif. Instruments*, vol. 7, pp. 653–

657, 1974.

[40] R. H. Leggatt, D. J. Smith, S. D. Smith, and F. Faure, “Development and experimental validation of the deep hole method for residual stress measurement,” *J. Strain Anal.*, vol. 31, no. 3, 1996.

[41] D. George, E. Kingston, and D. J. Smith, “Measurement of through-thickness stresses using small holes,” *J. Strain Anal.*, vol. 37, no. 2, pp. 125–139, 2002.

[42] A. H. Mahmoudi, S. Hossain, C. E. Truman, D. J. Smith, and M. J. Pavier, “A new procedure to measure near yield residual stresses using the deep hole drilling technique,” *Exp. Mech.*, vol. 49, pp. 595–604, 2009.

[43] D. M. Goudar, C. E. Truman, and D. J. Smith, “Evaluating uncertainty in residual stress measured using the deep-hole drilling technique,” *Strain*, vol. 47, pp. 62–74, 2011.

[44] M. B. Prime, “Cross-sectional mapping of residual stresses by measuring the surface contour after a cut,” *J. Eng. Mater. Technol.*, vol. 123, pp. 162–168, 2001.

[45] M. B. Prime, “Contour Method Advanced Applications: Hoop Stresses in Cylinders and Discontinuities,” in *Engineering Applications of Residual Stress, Volume 8, Proceedings of the 2011 Annual Conference on Experimental and Applied Mechanics*, 2011, vol. 8, pp. 13–29.

[46] F. Hosseinzadeh, P. Ledgard, and P. J. Bouchard, “Controlling the Cut in Contour Residual Stress Measurements of Electron Beam Welded Ti-6Al-4V Alloy Plates,” *Exp. Mech.*, vol. 53, no. 5, pp. 829–839, 2013.

[47] F. Hosseinzadeh and P. J. Bouchard, “Mapping Multiple Components of the Residual

Stress Tensor in a Large P91 Steel Pipe Girth Weld Using a Single Contour Cut," *Exp. Mech.*, vol. 53, pp. 171–181, 2013.

[48] A. T. DeWald and M. R. Hill, "Multi-Axial Contour Method for Mapping Residual Stresses in Continuously Processed Bodies," *Exp. Mech.*, vol. 46, no. 4, pp. 473–490, May 2006.

[49] P. Pagliaro, M. B. Prime, J. S. Robinson, B. Clausen, H. Swenson, M. Steinzig, and B. Zuccarello, "Measuring Inaccessible Residual Stresses Using Multiple Methods and Superposition," *Exp. Mech.*, vol. 51, no. 7, pp. 1123–1134, 2011.

[50] J. D. Pollard, S. Rahimi, A. Watford, M. Jackson, and B. P. Wynne, "The determination of residual stress in extruded Ti-6Al-4V by contour method and finite element analysis," in *Proceedings of the 13th World Conference on Titanium*, 2016, pp. 305–310.

[51] M. B. Prime and A. T. DeWald, "The Contour Method," in *Practical Residual Stress Measurement Methods*, John Wiley & Sons Ltd, 2013, pp. 109–138.

[52] G. Schnier, J. Wood, and A. Galloway, "An Experimental Validation of Residual Stresses in Weld Clad Pipelines," in *Research and Applications in Structural Engineering, Mechanics & Computation: Proceedings of the Fifth International Conference on Structural Engineering, Mechanics & Computation*, 2013, pp. 613–617.

[53] G. Schnier, J. Wood, and A. Galloway, "Investigating the Effects of Process Variables on the Residual Stresses of Weld and Laser Cladding," *Adv. Mater. Res.*, vol. 996, pp. 481–487, Aug. 2014.

[54] M. B. Prime and M. L. Steinzig, "Beyond the Streetlight Effect: A United Future for

Relaxation and Diffraction Methods for Residual Stress Measurement," *Adv. Mater. Res.*, vol. 996, pp. 234–242, Aug. 2014.

[55] K. Genel, M. Demirkol, and M. Çapa, "Effect of Ion Nitriding on Fatigue Behaviour of AISI 4140 Steel," *Mater. Sci. Eng. A*, vol. 279, no. 1–2, pp. 207–216, Feb. 2000.

[56] Y. Tomota, S. Daikuhara, S. Nagayama, M. Sugawara, N. Ozawa, Y. Adachi, S. Harjo, and S. Hattori, "Stress Corrosion Cracking Behavior at Inconel and Low Alloy Steel Weld Interfaces," *Metall. Mater. Trans. A*, Sep. 2014.

[57] S. Rahimi, K. Mehrez, and T. J. Marrow, "Effect of surface machining on intergranular stress corrosion cracking (IGSCC) in sensitised type 304 austenitic stainless steel," *Corros. Eng. Sci. Technol.*, vol. 51, no. 5, 2016.

[58] S. Rahimi and T. J. Marrow, "Effects of orientation, stress and exposure time on short intergranular stress corrosion crack behaviour in sensitised type 304 austenitic stainless steel," *Fatigue Fract. Eng. Mater. Struct.*, vol. 35, pp. 359–373, 2011.

[59] M. D. Olson, A. T. DeWald, M. B. Prime, and M. R. Hill, "Estimation of Uncertainty for Contour Method Residual Stress Measurements," *Exp. Mech.*, Dec. 2014.

[60] L. Singh, V. Shah, and N. K. Singh, "Study The Influence of TIG Welding Parameters On Weld Characteristics Of 5083 Aluminum Alloy," *Int. J. Eng. Sci. Innov. Technol.*, vol. 2, no. 5, pp. 462–468, 2013.

[61] J. E. S. Leal, T. F. Costa, and R. V. Arencibia, "Evaluation of Geometric Quality of Weld Beads in the Joining of Carbon Steel Pipelines with Single Pass," *J. Power Energy Eng.*, vol. 1, pp. 1–5, 2013.

[62] M. C. Smith and A. C. Smith, "NeT bead-on-plate round robin: Comparison of residual stress predictions and measurements," *Int. J. Press. Vessel. Pip.*, vol. 86, no. 1, pp. 79–95, 2009.

[63] M. Benachour, M. Benguediab, and N. Benachour, "Notch Fatigue Crack Initiation and Propagation Life under Constant Amplitude Loading through Residual Stress Field," *Adv. Mater. Res.*, vol. 682, pp. 17–24, Apr. 2013.

[64] P. Šohaj and V. Jan, "Local Changes of Microhardness in Dissimilar Weld Joints after High Temperature Exposure," *Key Eng. Mater.*, vol. 586, pp. 249–252, Sep. 2013.

[65] L. Pan, B. P. Athreya, J. A. Forck, W. Huang, L. Zhang, T. Hong, W. Li, W. Ulrich, and J. C. Mach, "Welding residual stress impact on fatigue life of a welded structure," *Weld. World*, vol. 57, no. 5, pp. 685–691, Jul. 2013.

[66] U. Zerbst, R. A. Ainsworth, H. T. Beier, H. Pisarski, Z. L. Zhang, K. Nikbin, T. Nitschke-Pagel, S. Münstermann, P. Kucharczyk, and D. Klingbeil, "Review on fracture and crack propagation in weldments – A fracture mechanics perspective," *Eng. Fract. Mech.*, vol. 132, pp. 200–276, 2014.

TABLE 1 Weld clad specimen dimensions.

Variable	Label	Measured value (mm)
Inner diameter	$Ø_{in}$	126.80
Cylinder length	L	193.32
Wall thickness	T	100.16
Bead depth	R_d	0.35

Bead width	R_w	3.40
Clad layer thickness		6

TABLE 2 Typical nominal chemical composition of 4330 alloy steel and IN625 welding wire.

4330		IN625	
Fe	95.3-98.1%	Ni	58% min.
Ni	1-1.5%	Cr	20-23%
Mn	≤1%	Mo	8-10%
Si	≤0.8%	Nb+Ta	3.15-4.15%
Cr	0.4-0.6%	Fe	5% max.
Mo	0.3-0.5%	Al	0.4% max.
C	0.2-0.3%	Ti	0.4% max.
		C	0.1% max.
		Mn	0.5% max.
		Si	0.5% max.
		Cu	0.5% max.
		P	0.015% max.
		S	0.015% max.

TABLE 3 Mechanical properties for clad and substrate materials, obtained experimentally.

	Yield Strength (MPa)	Young's Modulus (GPa)	Poisson's Ratio
IN625	474	168	0.29
4330	869	189.8	0.289

TABLE 4 Maximum tensile hoop and axial residual stresses and locations obtained using XRD, ESPI, DHD and CM.

	$\sigma_{hoop, max}$	Location from clad surface (mm)	$\sigma_{axial, max}$	Location from clad surface (mm)
XRD	222	0	117	0
ESPI	253	1.05	407	1.2
DHD	312	0.6	333	0.6
CM	406	0.37	266	1

TABLE 5 Maximum compressive hoop and axial residual stresses and locations obtained using XRD, ESPI, DHD and CM.

	$\sigma_{hoop, max}$	Location from clad surface (mm)	$\sigma_{axial, max}$	Location from clad surface (mm)
XRD	-546	0	-605	0
ESPI	-314	0.001	-191	0.051
DHD	-62	31	-113	18
CM	-130	1.9	-57	19.5

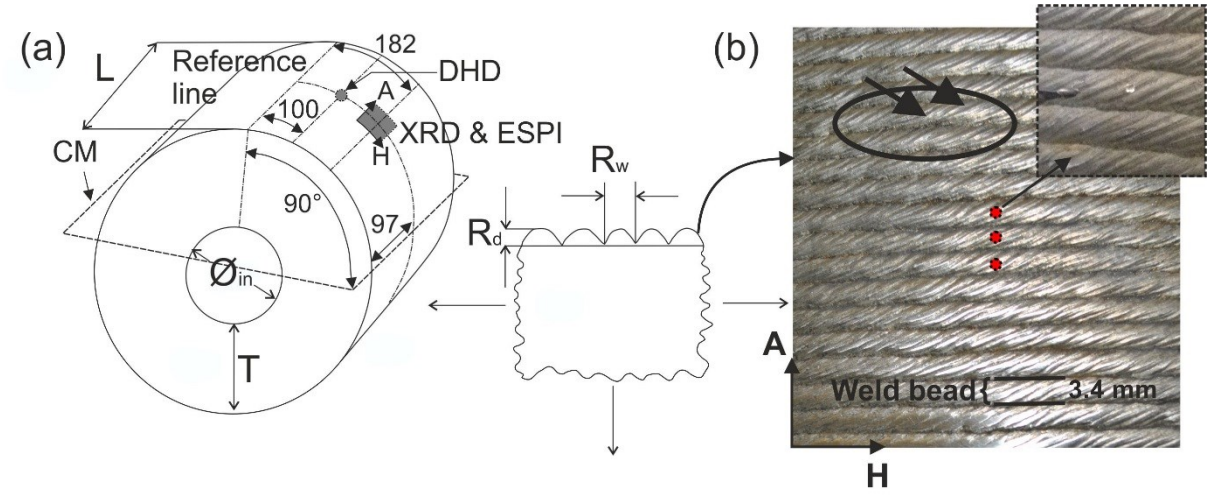

FIG. 1 (a) Schematic representation of weld clad cylinder detailing dimensions of interest, plane of cut for the contour method, measurement locations for XRD and ESPI and stress orientations (A and H being axial and hoop stresses respectively) (b) Illustration of weld surface with position of XRD (red circle) and ESPI (dashed circle) measurements, showing a magnified image of the position of a drilled hole to indicate the scale with respect to the weld bead, along with a schematic representation of the weld peaks and troughs.

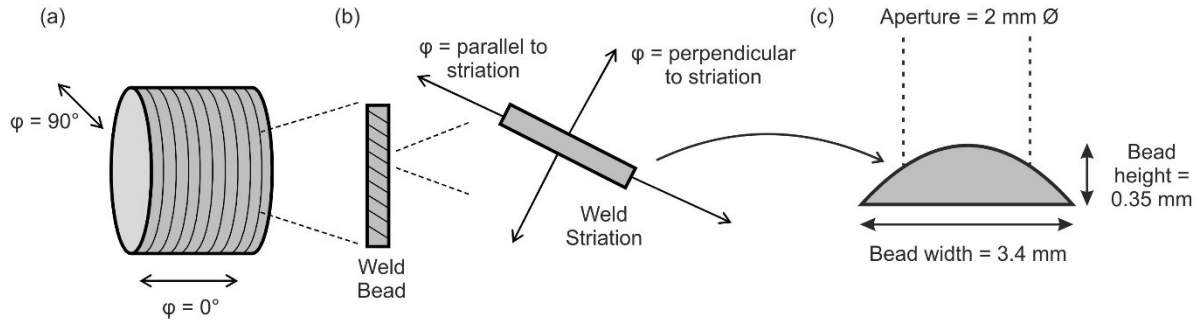

FIG. 2 (a) Orientation of φ-angles, during XRD stress measurements, with respect to the global component axes, (b) local weld beads and the arrangement of weld ripples within each bead, and (c) relation of weld bead geometry to the incident X-ray aperture.

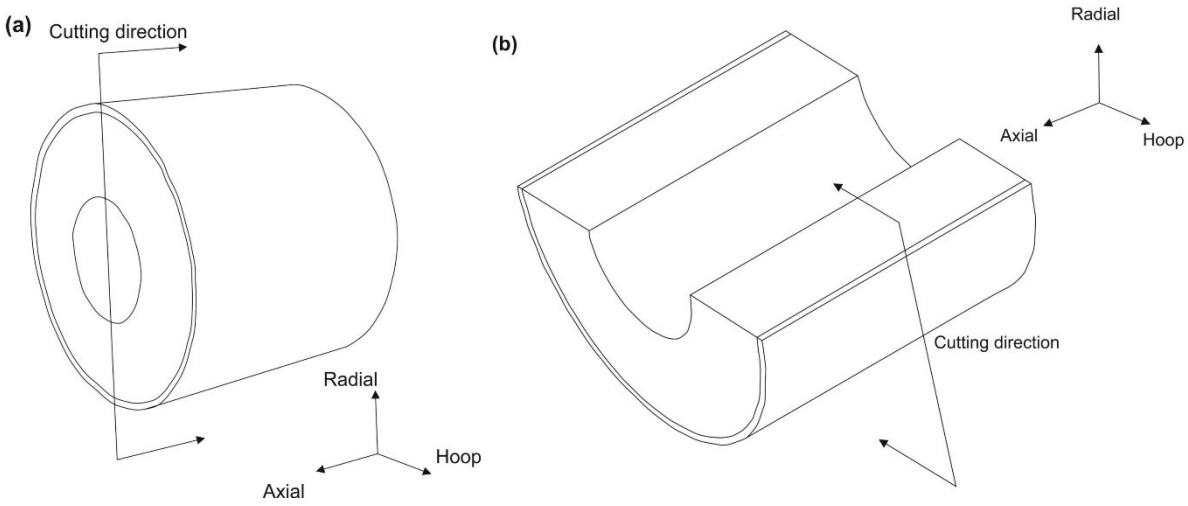

FIG. 3 Cutting directions to obtain (a) hoop and (b) axial stress components, figures indicating orientations of all stress components.

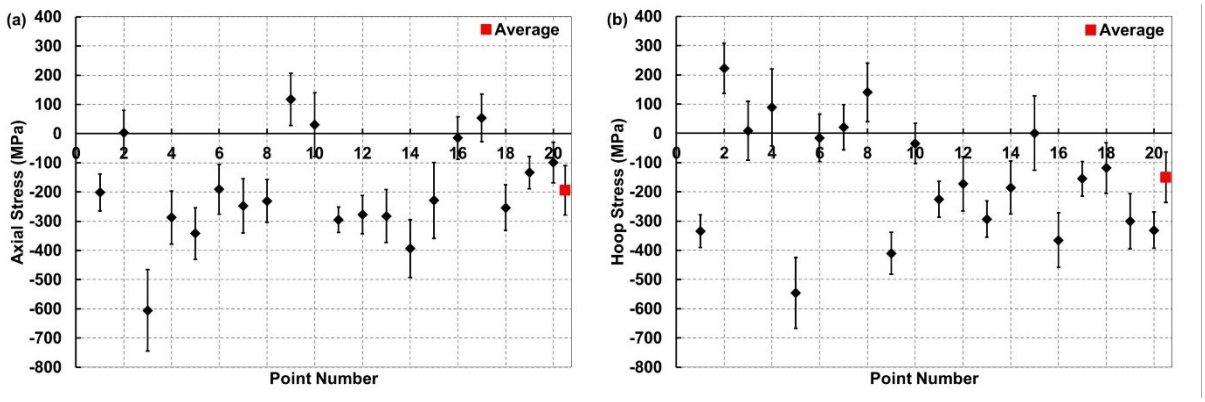

FIG. 4 (a) Axial and (b) hoop residual stresses measured on 20 consecutive weld bead peaks in IN625 as-clad surface using XRD.

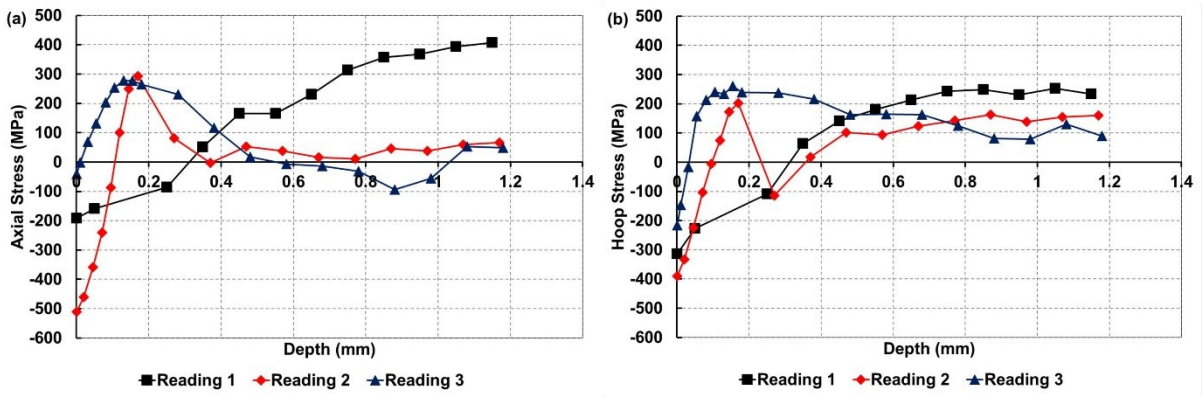

FIG. 5 (a) Axial and (b) hoop residual stresses measured on weld bead peaks in IN625 as-clad surface using ESPI.

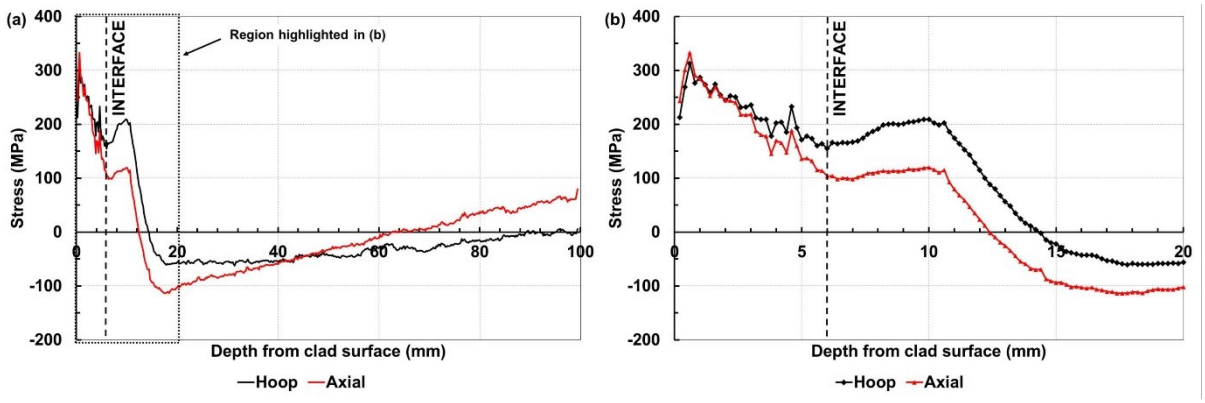

FIG. 6 Hoop and axial residual stresses (a) throughout cylinder (b) in region of clad, HAZ and substrate measured in IN625 clad cylinder using DHD.

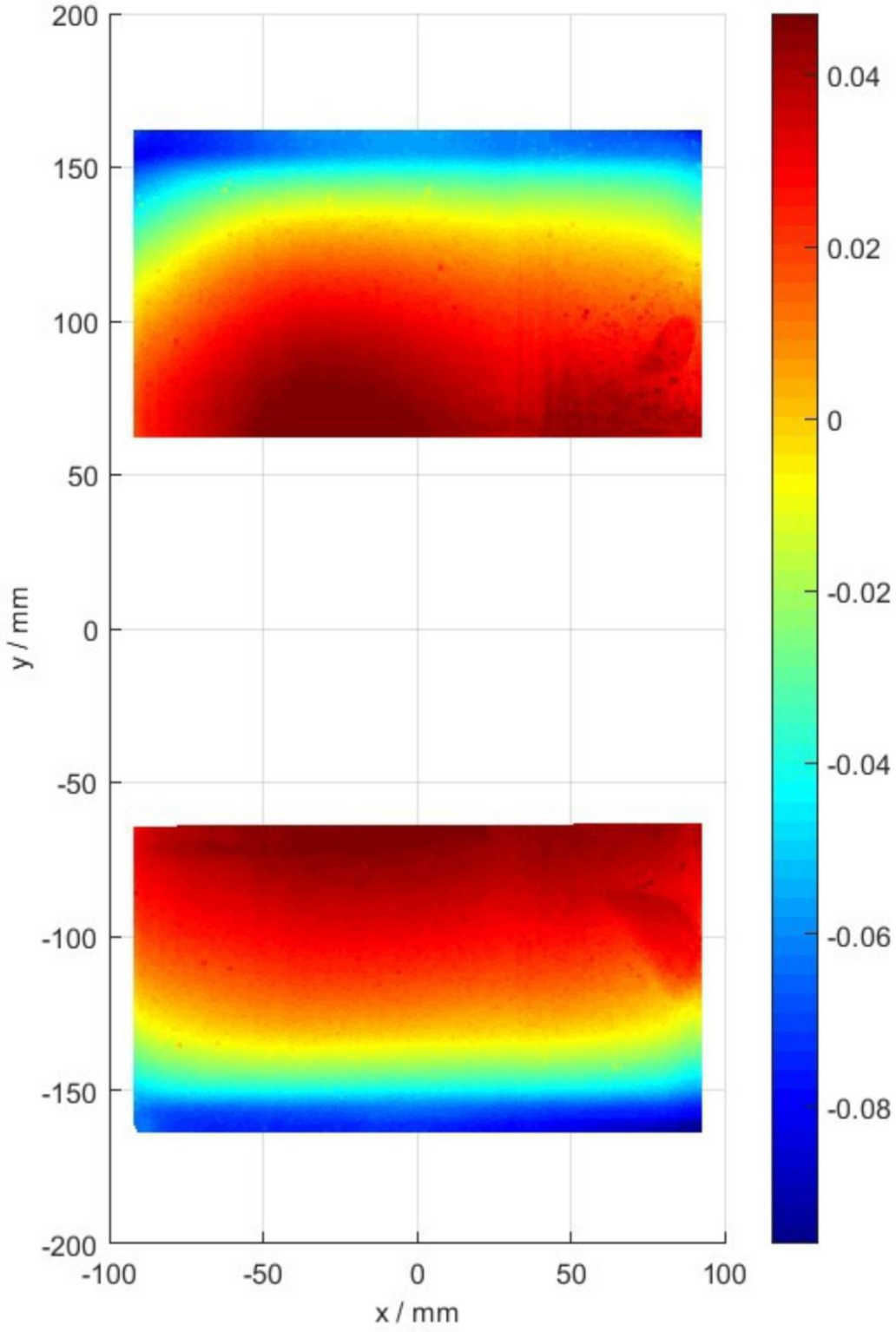

FIG. 7 Contour plot of the averaged surface height in millimetres obtained by the CMM for the hoop stress measurement.

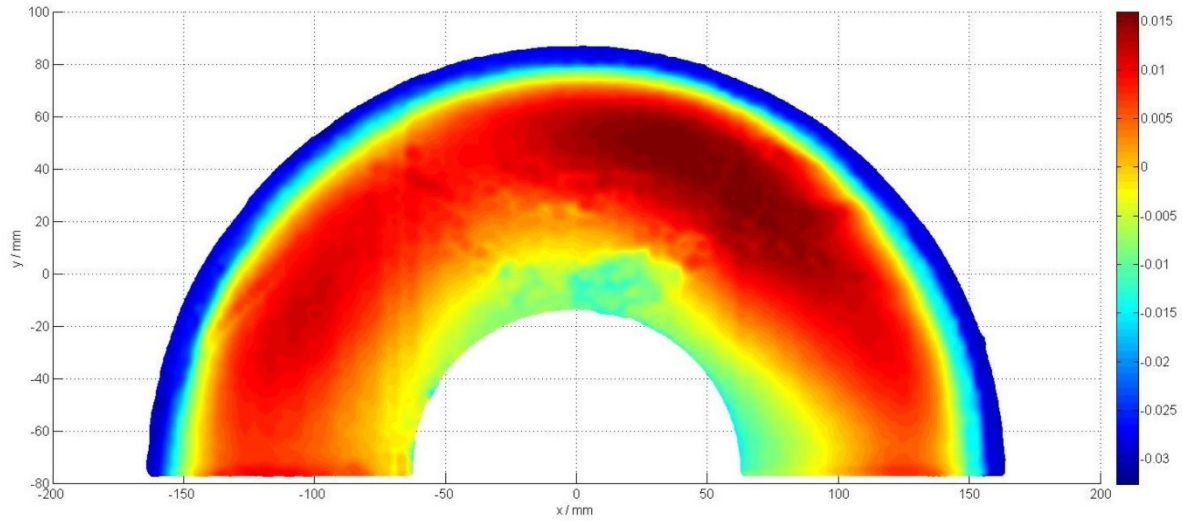

FIG. 8 Contour plot of the averaged surface height in millimetres obtained by the CMM for the axial stress measurement.

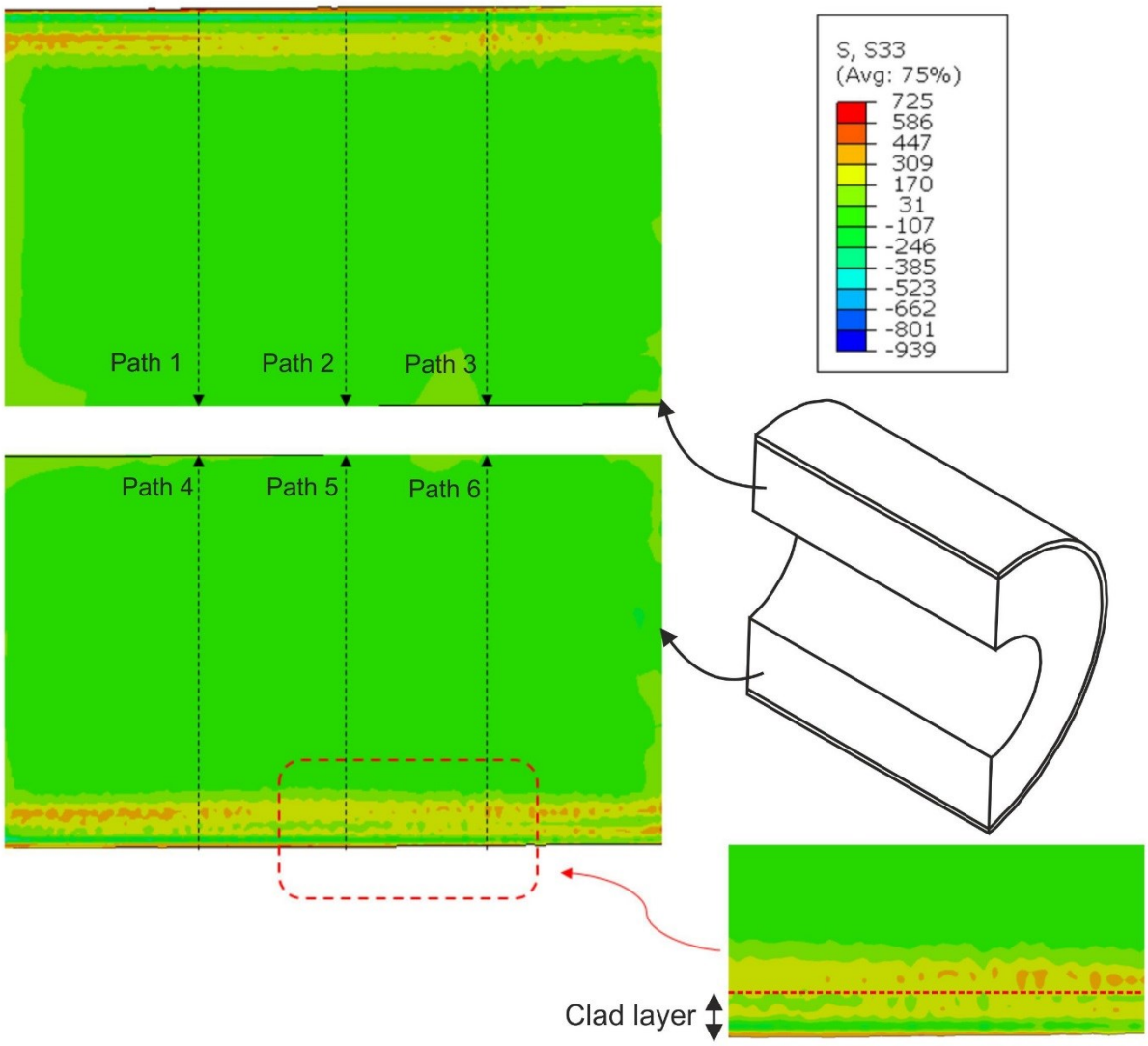

FIG. 9 Hoop residual stress (MPa) measured in IN625 clad cylinder using CM, illustrating paths utilised in FIG. 10.

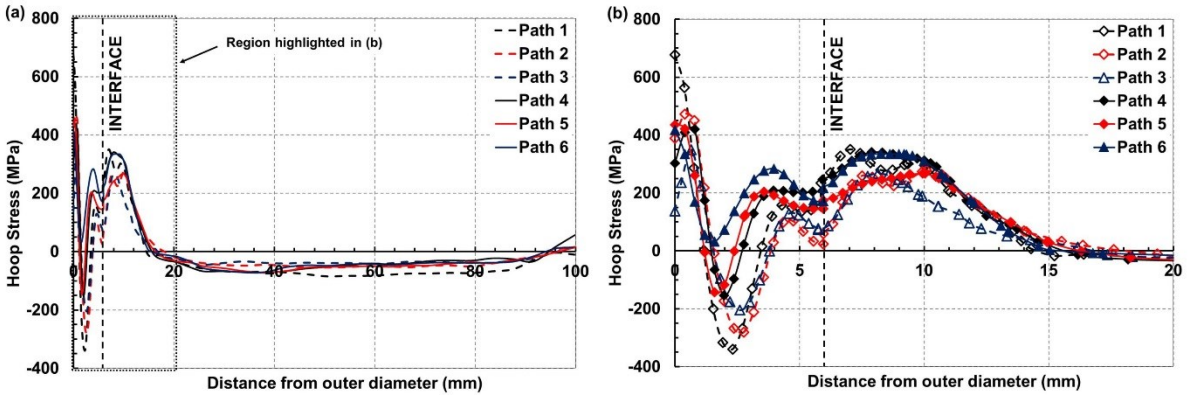

FIG. 10 Hoop residual stress profile (a) throughout the component, and (b) in a region of clad layer and HAZ in IN625 clad cylinder using CM plotted along six paths illustrated in FIG. 9.

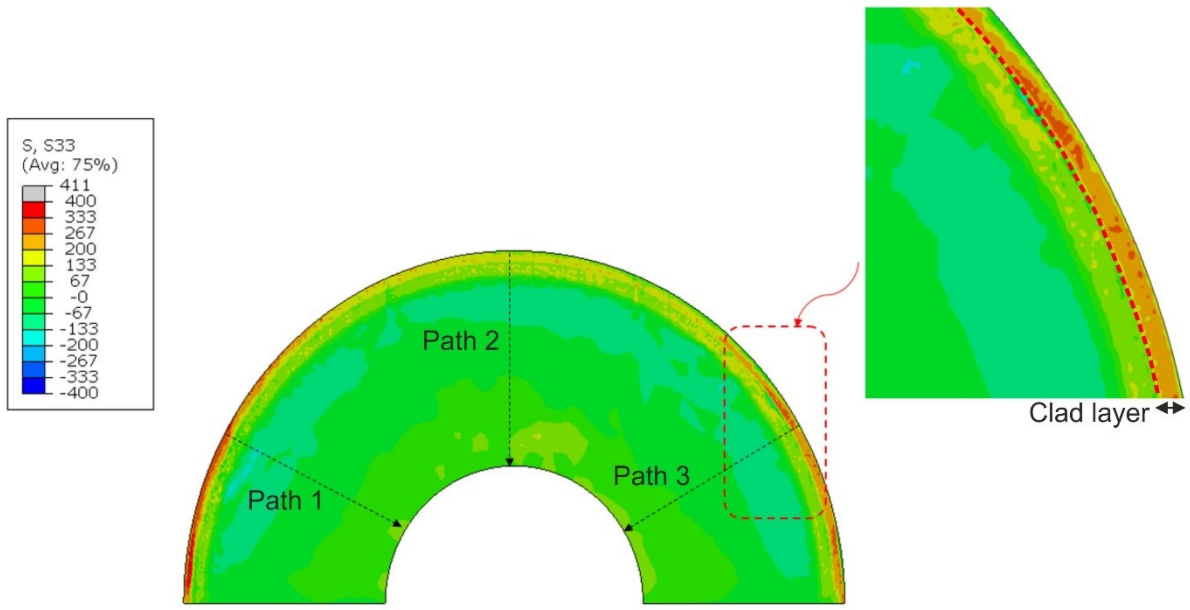

FIG. 11 Total axial residual stress (MPa) measured in IN625 clad cylinder using CM, illustrating paths utilised in FIG. 12.

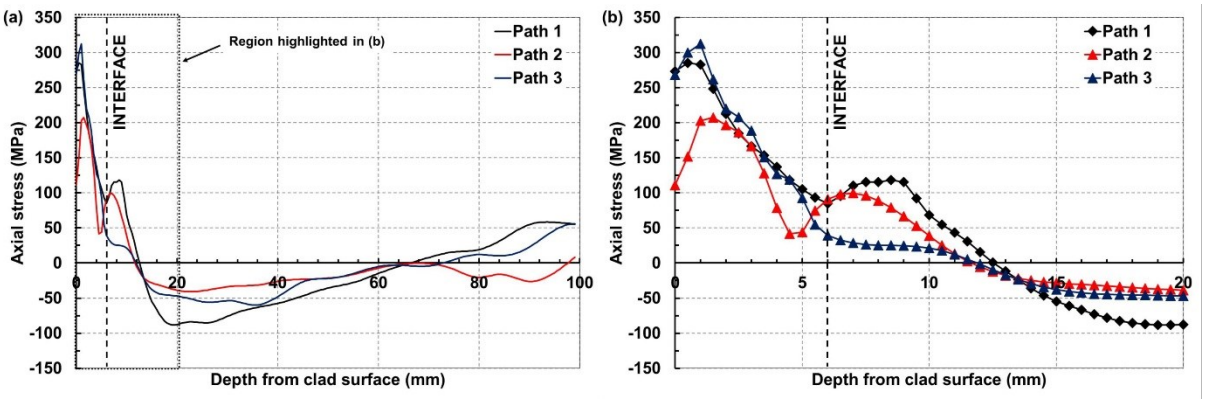

FIG. 12 Axial residual stress profiles (a) throughout the component, and (b) in a region of clad layer and HAZ in IN625 clad cylinder, measured using CM along the three paths illustrated in FIG. 11.

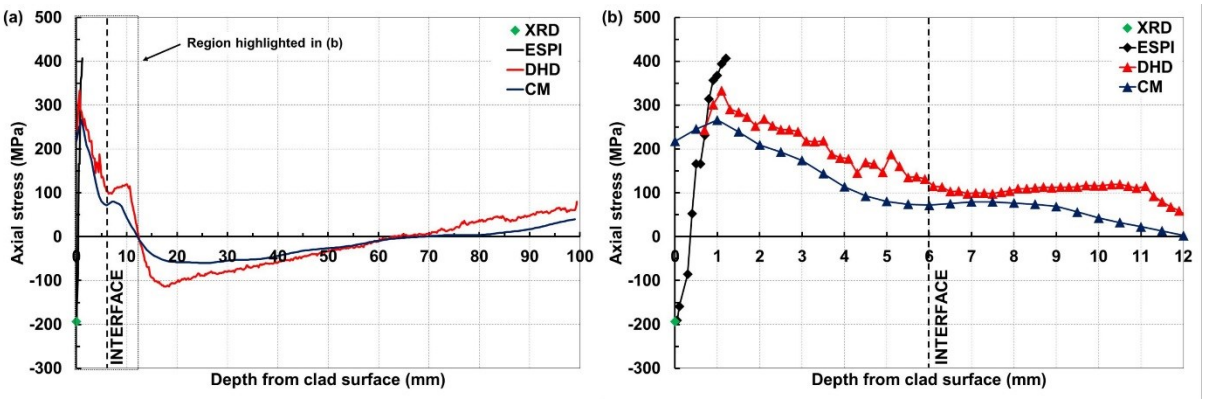

FIG. 13 Comparison of axial stress measured (a) throughout component (b) in region of clad layer and HAZ in IN625 clad cylinder using XRD, ESPI, DHD and CM.

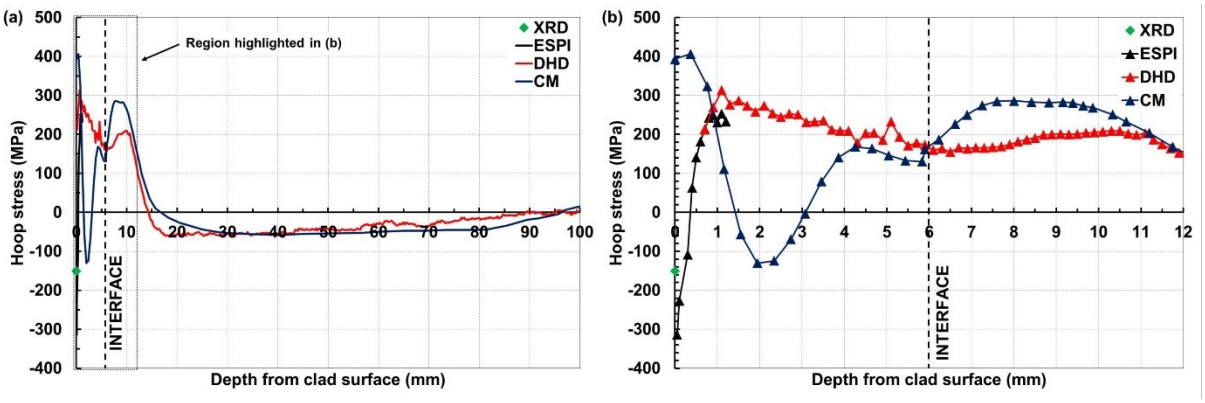

FIG. 14 Comparison of hoop stress measured (a) throughout component (b) in region of clad layer and HAZ in IN625 clad cylinder using XRD, ESPI, DHD and CM.